

A tunable UV spectrometer for Doppler broadening thermometry of mercury

Original

A tunable UV spectrometer for Doppler broadening thermometry of mercury / Clivati, Cecilia; Gravina, Stefania; Castrillo, Antonio; Costanzo, GIOVANNI A.; Filippoblevi, ; Gianfrani, Livio. - In: OPTICS LETTERS. - ISSN 0146-9592. - STAMPA. - 45:13(2020), pp. 3693-3696. [10.1364/OL.393793]

Availability:

This version is available at: 11583/2831054 since: 2020-06-26T09:03:44Z

Publisher:

Optical Society of America:2010 Massachusetts Avenue Northwest:Washington, DC

Published

DOI:10.1364/OL.393793

Terms of use:

This article is made available under terms and conditions as specified in the corresponding bibliographic description in the repository

Publisher copyright

Optica Publishing Group (formely OSA) postprint/Author's Accepted Manuscript

"© 2020 Optica Publishing Group. One print or electronic copy may be made for personal use only. Systematic reproduction and distribution, duplication of any material in this paper for a fee or for commercial purposes, or modifications of the content of this paper are prohibited."

(Article begins on next page)

A tunable UV spectrometer for Doppler broadening thermometry of mercury

CECILIA CLIVATI^{1,*}, STEFANIA GRAVINA², ANTONIO CASTRILLO², GIOVANNI A. COSTANZO^{1,3}, FILIPPO LEVI¹, AND LIVIO GIANFRANI²

¹Istituto Nazionale di Ricerca Metrologica (INRiM), Torino, Italy

²Department of Mathematics and Physics, Università degli Studi della Campania "Luigi Vanvitelli", Caserta, Italy

³Department of Electronics and Telecommunications, Politecnico di Torino, Torino, Italy

*Corresponding author: c.clivati@inrim.it

Compiled March 30, 2020

We realised a tunable UV laser source at 253 nm for Doppler-broadening thermometry on the 1S_0 - 3P_1 intercombination line in mercury vapors. Our setup is based on the two-stage second harmonic generation of a 1015 nm diode laser in a fiber-coupled periodically-poled lithium niobate waveguide crystal and a beta-barium borate crystal in enhancement cavity, and we exploit injection locking of a 507 nm diode laser to boost the available optical power after the first duplication. The realized source has 1×10^{-4} relative intensity stability, Gaussian shape and over 10 GHz mode-hop-free tunable range. These features are necessary for retrieving the thermodynamic temperature of the atomic sample from the absorption profile with 10^{-6} accuracy. This will make Doppler broadening thermometry a viable technique for the practical realization of the kelvin in the new International System of Units. © 2020 Optical Society of America

<http://dx.doi.org/10.1364/ao.XX.XXXXXX>

In the new International System of units (SI), the kelvin, unit of measurement of the thermodynamic temperature T , is defined in terms of a fixed value of the Boltzmann constant, $k_B = 1.380649 \times 10^{-23}$ J/K. Any method based upon a well-understood physical system, whose fundamental equation gives the thermal energy $k_B T$ as a function of other independent and measurable quantities, assumes the role of a primary method for the practical realization of the new kelvin [1, 2]. Among them, Doppler Broadening Thermometry (DBT) is widely recognized as a very promising technique, even though it has not yet reached the same accuracy as acoustic gas thermometry and dielectric-constant gas thermometry [3–5]. DBT is an optical route to the thermodynamic temperature determination that consists in measuring the Doppler width of a spectral line of an atomic or molecular gas sample at the thermodynamic equilibrium [6]. So far, the best results have been achieved probing the near-infrared (NIR) vibration-rotation spectrum of acetylene, with an overall uncertainty of 23 parts per million (ppm) for temperature determinations between the triple point of water and the gallium melting point [7].

Past literature shows a few examples of DBT implementations in which low-pressure alkali-metal vapors such as Rb and Cs atoms [8, 9] have

been used as thermometric substance. Mercury is an ideal candidate to perform DBT for a number of favourable reasons, not yet experienced so far. More particularly, the current limitations of DBT are likely to be overcome by probing the $6s^2\ ^1S_0 \rightarrow 6s6p\ ^3P_1$ intercombination transition at 253 nm, which is normally used for laser cooling [10–12]. DBT can be performed on both bosonic isotopes ^{200}Hg and ^{202}Hg ; the former nearby the triple point of water, the latter at lower temperatures. At the temperature of the triple point of water, the vapor pressure of mercury is sufficiently small to neglect the collisional broadening, but at the same time high enough to allow for the observation of the intercombination line with a good signal-to-noise ratio. In addition, thanks to the much simpler structure of the spectrum as compared to that of molecules, the line profile is poorly affected by nearby resonances and quantum interference effects, thus allowing accurate modelling [9, 13]. The ratio of the Doppler and natural width of the atomic transition is much more favourable for the selected Hg line as compared to that of Rb and Cs. Hence, interrogation with a sub-kHz-linewidth laser would allow approaching the ppm level in temperature determinations, making DBT a viable method for the realization of the new kelvin.

For the practical implementation of the method, the laser source must feature, in addition to a sub-kHz linewidth, absolute frequency traceability, continuous tunability over 6 GHz to ensure a sufficiently broad scanning region around the line center, relative intensity stability at the level of 10^{-4} and a high-quality spatial intensity profile. In particular, a TEM₀₀ mode would be desirable. On the other hand, few μW of optical power are sufficient. These requirements are more stringent and usually not shared with setups designed for laser cooling [10–12] and spectroscopy [14–16] of Hg, and call for dedicated solutions.

Here, we describe the realisation of a laser source for DBT of mercury at 253 nm which features these requirements and can be tuned continuously over more than 10 GHz. As a first demonstration, we performed Doppler-limited absorption spectroscopy of the intercombination transition of mercury isotopes, in a natural abundant sample. These measurements are preliminary to the realization of a primary thermometer based on DBT in mercury vapors.

Our setup is based on the second harmonic generation (SHG) of a 1015 nm diode laser using a periodically-poled lithium niobate (PPLN) crystal. The produced SHG beam seeds a diode laser at 507 nm, which is further duplicated in a beta-barium borate (BBO) crystal. A detailed sketch of the experimental apparatus is shown in Fig. 1. The master laser (DL1015) is an AR-coated diode (Toptica photonics LD-1060-

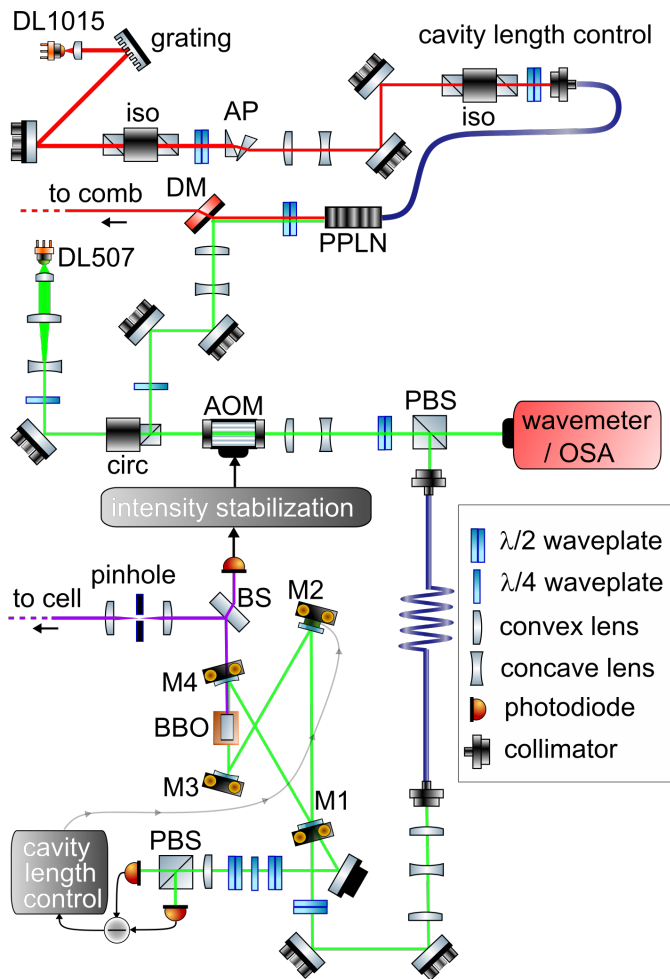


Fig. 1. A sketch of the optical setup. DL1015: master laser at 1015 nm; iso: isolators; AP: anamorphic prisms; PPLN: Periodically-poled Lithium Niobate crystal for first-stage duplication; DM: dichroic mirror; circ: circulator; DL507: slave diode laser at 507 nm; AOM: acousto-optic modulator; PBS: polarization beam-splitter; OSA: optical spectrum analyzer; M1: input mirror for second-stage duplication cavity; M2: piezo-actuated mirror; M3, M4: concave mirrors; BBO: crystal for second-stage duplication; BS: beam splitter.

0200-AR-2) emitting in the 960 nm–1060 nm region, mounted in an external cavity about 15 mm long and collimated with an aspheric lens with 6.24 mm focal length. Feedback is provided through a blazed grating with 2400 grooves/mm, which has a diffraction efficiency of 30% at 1015 nm when the beam polarization is vertical, namely parallel to the grating lines. About 65 mW of optical power are available at output when pumping with 320 mA. The laser can be tuned via the pump current with a sensitivity of 180 MHz/mA, via the temperature (sensitivity 18 GHz/K), or by tilting the grating, which is mounted on a piezo-actuator (sensitivity 680 MHz/V).

The first-stage duplication (1015 nm → 507 nm) is performed in a fiber-coupled PPLN crystal in waveguide (NTT), which is a robust, alignment-free solution [17, 18]. About 55% of the optical power is coupled to the crystal by correcting the beam ellipticity, about 2.1, with an anamorphic prism pair (AP). Two optical isolators protect the master laser from backreflections occurring on the crystal facets and coupling back into the optical fiber, which would otherwise destroy the cavity mode. For the considered optical power, the measured crystal

efficiency is $(1.8 \pm 0.2) \text{W}^{-1}$ and about 3 mW of green light are available at the output. The efficiency is optimized by adjusting the crystal temperature, and decreases by less than 3% when the laser frequency is tuned by 2 GHz, which ensures that no active temperature tuning is required on the crystal to maintain the quasi-phasematch condition during the scan. A dichroic mirror (DM) extracts the unconverted NIR radiation, which will be sent to an optical comb for frequency referencing.

The produced radiation at 507 nm seeds a high-power diode laser (DL507) at the same wavelength (Nichia NDE4116) [15, 19–21]. Injection locking boosts the optical power available for the second-stage duplication and strongly attenuates the power variations at the PPLN output occurring during the frequency scan. These are due to power variations of the master laser, efficiency loss of the crystal and coupling loss into the fiber as the beam orientation and the driving current of the master laser change. The green laser has no AR-coating and exhibits multi-mode emission, with modes separation of ~ 60 GHz. It produces about 80 mW optical power when pumped with 168 mA. The slave laser is mode-matched to the seeding beam using an aspherical collimation lens with focal length of 6.24 mm and a cylindrical telescope to correct its ~ 2.2 ellipticity. In this condition, injection lock at the minimum seed power (0.9 mW) is achieved by simply overlapping the beam paths. Raising the seed power to 1.5 mW guarantees stable and single-mode operation for several hours. The slave laser passes through an acousto-optic modulator (AOM) which is used to stabilise the power, then coupled to a polarization-maintaining optical fiber for mode cleaning, with $>50\%$ coupling efficiency.

The second duplication (507 nm → 253 nm) is performed with a BBO crystal (Crestech) cut at $\theta=51.2^\circ$, housed in a bow-tie cavity with folding angle $\alpha/2=14^\circ$. The crystal is AR-coated at 507 nm and at 253 nm and is 12 mm long. According to the Boyd-Kleyman formula [22], the cavity should be designed with a beam waist of 19 μm in the crystal. However, due to the high walk-off $\rho=84.7$ mrad of BBO, it is preferable to operate with a larger waist on the horizontal plane. Similarly to what has been described in [16], we designed the cavity [23] to have a waist of 30 μm in the horizontal plane, while on the vertical plane the waist is maintained at its optimal value. The cavity has two plane mirrors (M1 and M2) and two concave mirrors (M3 and M4) with radius 75 mm and is 340.8 mm long, which leads to a free-spectral-range of 880 MHz. The input mirror M1 has nominal reflectivity $R_1=0.986$, designed to optimize the coupling [24], while mirrors M2–M4 have reflectivity $R_2, R_3, R_4 > 0.999$ at 507 nm. The fundamental beam is coupled to the secondary waist using a spherical telescope and a cylindrical lens. The BBO crystal is mounted on a rotatable platform for phase-matching optimization and is placed inside an oven. Although birefringent phase-matching is achieved by angle-tuning only, the crystal is temperature-stabilized at 50 °C to prevent water vapour deposition and reduce degradation [16]. The cavity is locked to the incoming beam through the Hänsch-Couillaud technique [25], by moving the piezo-actuated mirror M2. The mechanical resonance of the system is 20 kHz, which ensures a tight lock of the cavity in absence of anomalous acoustic noise.

The produced UV power was measured on a silicon carbide (SiC) photodiode with an area of $\sim 0.7 \text{mm}^2$ and narrowband sensitivity in the UV-C spectral domain. The photodiode responsivity is 0.08 A/W at 253 nm and $< 8 \times 10^{-9}$ A/W at 507 nm, which ensures sufficient blindness to stray light at the fundamental wavelength. By performing a quadratic fit of the produced UV power versus incident power in a single pass, we estimated an efficiency of $\eta = (5.7 \pm 0.3) \times 10^{-5} \text{W}^{-1}$ for the BBO crystal. Fig. 2 shows the UV power produced in the cavity setup. The second-harmonic beam power P_{SHG} generated inside the cavity can be written in terms of the fundamental beam power (P_{inc}) as

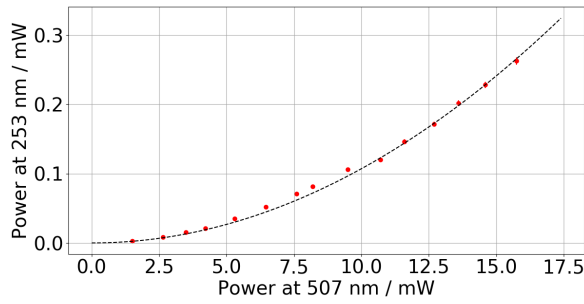


Fig. 2. Power at 253 nm produced by SHG in a BBO crystal with a cavity-enhanced setup, as a function of pump power at 507 nm.

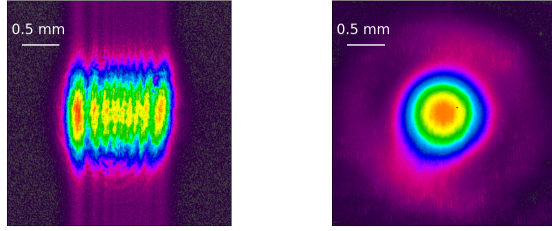


Fig. 3. a) Spatial profile of the UV beam as it exits the cavity, and b) when a mode-cleaning stage is added.

[24]:

$$P_{\text{SHG}} = \eta c_0^2 \frac{(1 - R_1)^2}{(1 - \sqrt{R_1(1 - I_{\text{cav}})})^4} P_{\text{inc}}^2 \quad (1)$$

Here, $I_{\text{cav}} = 1 - R_2 R_3 t_{\text{AR}}^2 \alpha_{507} R_4$ includes all optical losses of the setup except for those due to second-harmonic generation, namely, the reflectivity of cavity mirrors, the transmission t_{AR} on the input and output facets of the BBO crystal at 507 nm, and the crystal absorption α_{507} . c_0 represents the mode-matching coefficient and was estimated by comparing the measured ratio of reflected (P_{refl}) versus incident power with the expected one:

$$\frac{P_{\text{refl}}}{P_{\text{inc}}} = \frac{\sqrt{R_1} - \sqrt{1 - I_{\text{cav}}}}{(1 - \sqrt{R_1(1 - I_{\text{cav}})})^2} \quad (2)$$

The discrepancy between the two accounts for the fact that a fraction $(1 - c_0)$ of the incident power is reflected at MI due to mode-mismatch. Eq. 1 does not include the nonlinear loss term due to second harmonic generation, as this latter accounts for an additional loss of $\sim 10^{-4}$, which is negligible compared to the linear term. For this reason, the linear behaviour which is typically observed in second-harmonic generation crystals at high pump powers [16, 26, 27] is not appreciated in this case. The dashed line shows the expected power obtained for a resonator with $I_{\text{cav}} = 3.9 \times 10^{-3}$, which is consistent with the specified losses of the optical components as provided by the manufacturer. Based on this value, the coupling ratio for our setup was estimated to be $c_0 = 78\%$. Up to $250 \mu\text{W}$ of UV light are obtained at the maximum pump power of 15 mW.

Although the slave laser produces up to 80 mW when the driving current is 168 mA, the power available on the input coupler is limited by the insertion losses of circulator, AOM and optical fiber.

Fig. 3 (a) shows the far-field spatial profile of the UV beam after collimation, which is strongly affected by the BBO walk-off. Such an intensity profile is not suitable for DBT as its effect on the absorption

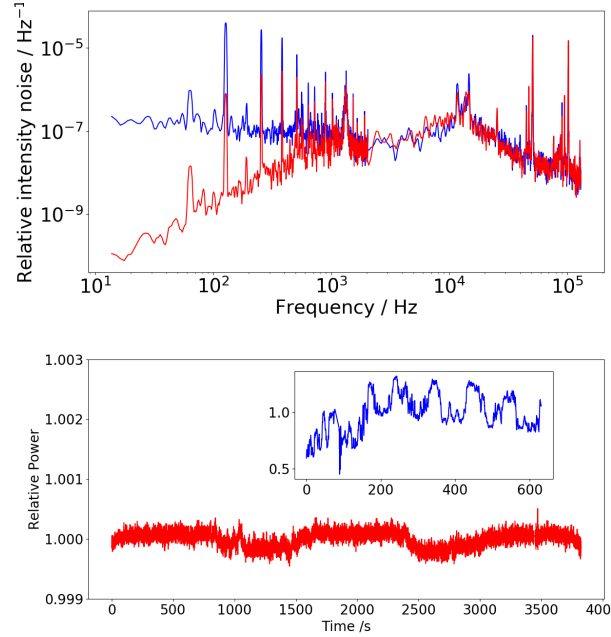


Fig. 4. Top: power spectral density of the relative intensity noise at 253 nm in an unstabilised (blue) and stabilised (red) condition. Bottom: relative intensity variations on the long-term in a stabilised condition (red). The inset shows typical power variations when power stabilization is not activated (blue).

linewidth of the atomic vapor cannot be properly modelled, thus increasing the overall uncertainty of the method. The mode quality was improved by strongly focusing the beam with a $f = 50$ mm lens. A $50 \mu\text{m}$ pinhole was placed at the beam waist and aligned using a 3-axes stage. About 20% of optical power is still available in the transmitted mode, which is enough for our application. Fig. 3 (b) shows the spatial profile measured in the far field after collimation with a $f = 200$ mm lens. The resulting beam shape can be more easily modelled so that its impact in the lineshape evaluation becomes negligible.

50% of the produced UV radiation is sent to a $60 \mu\text{m}^2$ area SiC photodiode for detecting power variations. These are compensated by adjusting the RF power driving the AOM at 507 nm. Fig. 4 (top graph) shows the power spectral density of the relative intensity noise in an unstabilised (blue) and stabilised (red) condition. An increase in the relative intensity noise is observed at about 20 kHz, which is due to frequency-to-amplitude conversion in correspondence of the locking bandwidth of the cavity. The bandwidth of the intensity control loop is intentionally limited to 1 kHz to avoid cross-talk between the two.

Fig. 4 (bottom graph) shows the long-term power variations in a stabilised (red) and unstabilised condition (blue, inset). Over 30% relative power variations are observed on the system when the stabilisation is not active. When stabilisation is activated, the relative variations are reduced to 4×10^{-5} over timescales of few minutes, which is the typical duration of a full scan. On the long term, a residual effect of the air-conditioning system, which has a cycle time of about 1500 s in our laboratory, is still visible and leads to maximum relative deviations from the nominal value of 1×10^{-4} . These performances fully meet the requirement for this experiment, as their impact on the absorption lineshape is already negligible, and could be further improved by passively insulating the system from the laboratory environment.

The operation of the UV source was verified by observing the shape of the intercombination transition for the ^{202}Hg bosonic isotope. The spectroscopic cell, not shown in Fig. 1, was 20 mm-long, sealed at the two

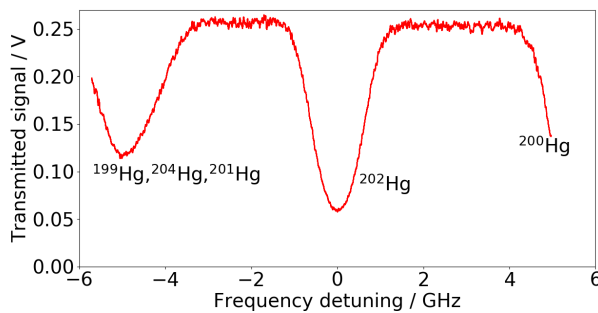


Fig. 5. Absorption spectrum of the Hg cell across the ^{202}Hg intercombination line.

ends by a pair of wedged AR-coated quartz windows and filled with Hg vapors, temperature-stabilised at the triple point of water. To do so, it was placed in a hollow copper block, in turn housed inside a cylindrical stainless-steel vacuum chamber. The temperature of the block was measured by a pair of precision platinum resistance thermometers (Pt100) and actively stabilized by means of four Peltier elements driven by a proportional integral derivative controller. As a result, the temperature was uniform and constant within 0.01 K. A SiC photodiode was used to measure the transmitted UV radiation while scanning the frequency of the laser source. To this purpose, the frequency of the NIR master laser was continuously tuned by applying a low-frequency ramp to the piezo actuator tilting the grating. Simultaneously, additional current was sent to the slave laser at 507 nm in a feed-forward scheme, so that injection from the seed light could be maintained throughout the full frequency scan. Fig. 5 shows an example of the absorption spectrum which can be obtained with a continuous scan. It shows the ^{202}Hg absorption profile along with a portion of the ^{200}Hg peak at higher frequency detuning, and the convolution of the ^{204}Hg transition and hyperfine structure components of the fermionic isotopes ^{199}Hg and ^{201}Hg at lower frequencies. More than 10 GHz continuous scan was possible without mode hopping, while maintaining the single-mode emission. The mode-hop-free tunable range of the UV laser is currently limited by that of the master laser, and could be further increased by applying the feed-forward approach also to the master laser current. Nevertheless, the achieved tunability already allows scanning a broad range around the target absorption line, which is more than enough for the aims of DBT.

In conclusion, we realised a laser source at 253 nm for DBT on the intercombination line of bosonic Hg isotopes. Although our application requires a UV optical power as low as few μW , other features such as a broad tuning range, high intensity stability and a Gaussian profile are crucial to allow retrieving the absolute temperature from the absorption profile with ppm accuracy. Such features can be easily achieved with our setup. It is worth noting that, being based on a master laser at 1015 nm, the UV spectrometer can be easily referenced to an SI-traceable frequency standard by direct stabilization of the master laser to a fiber optical frequency comb, whose power at this wavelength allows beatnote detection with sufficient signal-to-noise ratio. This will ensure sub-kHz-linewidth and a controlled frequency scan. This approach is combined with the advantages of newly-developed visible diode lasers, which have been recently demonstrated in spectroscopy applications [14, 15]. Thanks to injection lock of one of these lasers, we could increase the optical power over that available with a simple cascaded SHG scheme, and achieve the target relative intensity stability of 1×10^{-4} . These features, together with the compensation of BBO walk-off through efficient spatial filtering, make our spectrom-

eter suitable for primary gas thermometry, providing an optical method for the practical realization of the new kelvin.

FUNDING

This work is being performed within the frame of a National project funded by the Italian Ministry for Education and Research, entitled "A new primary method of gas thermometry based upon Doppler-broadened mercury spectroscopy in the UV region" (MIUR, PRIN2015 Call, Project n. 20152MRAKH).

DISCLOSURES

The use of trade names in this article is inserted for completeness and does not constitute an endorsement by the authors. The authors declare no conflicts of interest.

REFERENCES

- G. Machin, *Meas. Sci. Technol.* **29**, 022001 (2018).
- B. Fellmuth, J. Fischer, G. Machin, S. Picard, P. Steur, O. Tamura, R. White, H. Yoon, *Phil. Trans. R. Soc. A* **374**, 20150037 (2016).
- M. R. Moldover, R. M. Gavioso, J. B. Mehl, L. Pitre, M. de Podesta and J. T. Zhang, *Metrologia* **51**, 1 (2014).
- L. Pitre, F. Sparasci, L. Risehari, C. Guianvarch, C. Martin, M. E. Himbert, M. D. Plimmer, A. Allard, B. Marty, P. A. Giuliano Albo, B. Gao, M. R. Moldover and J. B. Mehl, *Metrologia* **54**, 856 (2017).
- Ch. Gaiser, Th. Zandt and B. Fellmuth, *Metrologia* **52**, 5 (2015).
- L. Gianfrani, *Philos. Trans. R. Soc. A* **374**, 20150047 (2016).
- A. Castrillo, E. Fasci, H. Dinesan, S. Gravina, L. Moretti, and L. Gianfrani, *Physical Review Applied* **11**, 064060 (2019).
- G.-W. Truong, E. F. May, T. M. Stace, and A. N. Luiten, *Phys. Rev. A* **83**, 033805 (2011).
- G.-W. Truong, J. D. Anstie, E. F. May, T. M. Stace, A. N. Luiten, *Nat. Comm.* **6**, 8345 (2015).
- J. J. McFerran, L. Yi, S. Mejri, S. Bize, *Opt. Lett.* **35**, 3078 (2010).
- H. Hachisu, K. Miyagishi, S. G. Porsev, A. Derevianko, V. D. Ovsiannikov, V. G. Pal'chikov, M. Takamoto, and H. Katori, *Physical Review Letters* **100**, 053001 (2008).
- M. Witkowski, G. Kowzan, R. Munoz-Rodriguez, R. Ciurylo, P. S. Z., P. Maslowski, M. Zawada, *Opt. Expr.* **27**, 11069 (2019).
- M. Horbatsch, E. A. Hessels, *Phys. Rev. A* **82**, 0521519-1-6 (2010).
- G. Almog, M. Scholz, W. Weber, P. Leisching, W. Kaenders, Th. Udem, *Rev. Sci. Instrum.* **86**, 033110 (2015).
- J. Alnis, U. Gustafsson, G. Somesfalean, and S. Svanberg, *Appl. Phys. Lett.* **76**, 1234 (2000).
- M. Scheid, F. Markert, J. Walz, J. Wang, M. Kirchner, and T. W. Haensch, *Opt. Lett.* **32**, 955 (2007).
- D. Akamatsu, M. Yasuda, T. Kohno, A. Onae, F.-L. Hong, *Opt. Expr.* **19**, 20476-2051 (2011).
- N. Chiodo, F. Du Burck, J. Hrabina, Y. Candela, J.-P. Wallerand, O. Acef, *Opt. Commun.* **311**, 239 (2013).
- C. J. H. Pagett, P. H. Moriya, R. Celistrino Teixeira, R. F. Shiozaki, M. Hemmerling, and Ph. W. Courteille, *Rev. Sci. Instr.* **87**, 053105 (2016).
- T. Hosoya, M. Miranda, R. Inoue, M. Kozuma, *Rev. Sci. Instr.* **86**, 073110 (2015).
- Y. Shimada, Y. Chida, N. Ohtsubo, T. Aoki, M. Takeuchi, T. Kuga, Y. Torii, *Rev. Sci. Instr.* **84**, 063101 (2013).
- G. D. Boyd and D. A. Kleinman, *J. Appl. Phys.* **39**, 3597 (1968).
- T. Freearde and C. Zimmermann, *Opt. Commun.* **199**, 435 (2001)
- W. P. Risk, T. R. Gosnell, and A. V. Nurmikko, *Compact Blue-Green Lasers* (Cambridge University, 2003)
- T. Haensch and B. Couillaud, *Opt. Commun.* **35**, 441 (1980)
- M. Pizzocaro, D. Calonico, P. Cancio Pastor, J. Catani, G. A. Costanzo, F. Levi, L. Lorini, *Appl. Opt.* **53**, 3388 (2014).
- R. Steinborn, A. Koglbauer, P. Bachor, T. Diehl, D. Kolbe, M. Stappel, J. Walz, *Opt. Expr.* **21**, 22693 (2013)